Fine-tuning of Side-chain Orientations on Nonfullerene Acceptors Enables Organic Solar Cells with 17.7% Efficiency

Gaoda Chai,‡[ab] Yuan Chang,‡[ab] Jianquan Zhang,*‡[ab] Xiaopeng Xu,[c] Liyang Yu,[c] Xinhui Zou,[abd] Xiaojun Li,[ab] Yuzhong Chen,[ab] Siwei Luo,[ab] Binbin Liu,[e] Fujin Bai,[ab] Zhenghui Luo,[ab] Han Yu,[ab] Jiaen Liang,[ab] Tao Liu,[ab] Kam Sing Wong,[d] Hang Zhou,[e] Qiang Peng*[c] and He Yan*[abf]

[a] Hong Kong University of Science and Technology-Shenzhen Research Institute, No. 9 Yuexing first RD, Hi-tech Park, Nanshan, Shenzhen 518057, P. R. China.

[b] Department of Chemistry, Guangdong-Hong Kong-Macao Joint Laboratory of Optoelectronic and Magnetic Functional Materials, Energy Institute and Hong Kong Branch of Chinese National Engineering Research Center for Tissue Restoration & Reconstruction, Hong Kong University of Science and Technology, Clear Water Bay, Kowloon, Hong Kong, P. R. China.

[c] School of Chemical Engineering, and State Key Laboratory of Polymer Materials Engineering, Sichuan University, Chengdu 610065, P. R. China.

[d] Department of Physics, Hong Kong University of Science and Technology, Clear Water Bay, Kowloon, Hong Kong, P. R. China.

[e] School of Electronic and Computer Engineering, Peking University Shenzhen Graduate School, Shenzhen 518055, P. R. China.

[f] Institute of Polymer Optoelectronic Materials and Devices, State Key Laboratory of Luminescent Materials and Devices, South China University of Technology (SCUT), Guangzhou 510640, P. R. China.

* E-mail: jzhangbn@connect.ust.hk (Z.J.), qiangpengjohnny@yahoo.com (P.Q.), hyan@ust.hk (H.Y.).

‡The first three authors contributed equally to this paper.

Abstract

Side-chain engineering has been shown to be an important strategy to optimize Y-series nonfullerene acceptors (NFAs). Most previous reports were focusing on changing the branching positions and size of the alkyl side chains on Y6. In this paper, we investigate the influence of the orientation of side chains on the properties of NFAs and the performance of the organic solar cells (OSCs). Three isomeric NFAs named *o*-BTP-PhC6, *m*-BTP-PhC6, and *p*-BTP-PhC6 are designed by changing the substitution positions and thus orientations of the side chains attached to the central core. Our studies show that the optimal side-chain orientation can be achieved by the meta-positioned hexylphenyl group (of the *m*-BTP-PhC6 molecule), which introduces significant beneficial effects on optical absorption, intermolecular packing and phase separation of the NFAs. By pairing a donor polymer PTQ10 with *m*-BTP-PhC6, device efficiencies of 17.7% can be achieved, which is among the best values for PTQ10-based nonfullerene OSC devices so far. These results reveal that regulating side-chain orientations of Y-series NFAs is a promising strategy to achieve favorable morphology, high charge mobility and solar cell performances.

Keywords: organic solar cells, non-fullerene acceptors, side-chain orientation, isomerization

Broader context

Non-fullerene acceptors (NFAs) have become one of the most important research topics in the field of organic solar cells (OSCs), due to their highly tunable optoelectronic and morphological properties. Recently, the rapid development of Y-series NFAs has enabled a paradigm shift in the OSC field with the device efficiencies exceeding 17%. Among various chemical modifications on Y-series NFAs, side-chain engineering is a facile and versatile strategy to manipulate intermolecular packing, blend film morphology and processability of the materials. However, current side-chain engineering of Y-series NFAs mainly focuses on the variations of the length, shape or branching positions of the side chains, and there are few studies on the side-chain orientations. In this work, three isomeric NFAs named *o*-BTP-PhC6, *m*-BTP-PhC6 and *p*-BTP-PhC6, respectively, were designed with different side-chain orientations. It is found that appropriate side-chain orientations are beneficial for optical absorption, intermolecular packing, and phase separation of NFAs. Encouragingly, by pairing PTQ10 as the electron donor, PTQ10:*m*-BTP-PhC6 achieves an outstanding PCE of 17.7%, which is among the best values for PTQ10-based devices reported to date. Our results open a new avenue for the side-chain engineering of Y-series NFAs by regulating side-chain orientations to achieve optimal morphology and high performance.

Introduction

Great strides have been made in the field of organic solar cells (OSCs) towards practical applications of optoelectronic devices.[1-7] OSCs not only rival many inorganic counterparts in terms of device performances but also offer numerous advantageous features such as lightweight, solution processing, and potentials in portable and flexible panels.[8-21] During the past five years, the power conversion efficiencies (PCE) of OSCs have increased to beyond 17%, by virtue of the emergence of highly performing nonfullerene acceptors (NFAs) with high tunability in chemical structures, optoelectronic properties and molecular packing.[22-29] So far, the state-of-the-art NFAs are the Y-series molecules featuring an A'-DAD-A' structure that delivered 15.7% efficiency when combining with a wide-bandgap donor polymer named PBDB-TF in the original report.[30-32] Subsequently, the research community encouraged by this result have achieved successive breakthroughs in harvesting the full potential of NFAs by fine-tuning of the molecular structure,[33-39] matching with donor polymers,[40-45] device engineering,[46-59] and in-depth studies on molecular packing and fundamental aspects.[60-65]

Among various molecular design strategies of Y-series NFAs, the side-chain modification plays a vital role in controlling the nanoscale morphology of the active layers and thereby device performances.[66-70] It can be found that the Y-series NFAs possess two sets of alkyl chains with the inner pair located on the pyrrole rings and the outer pair flanking at the β-positions of the thienothiophene moieties. Examples of side-chain engineering of Y-series NFAs began with the prolongation of the inner 2-ethylhexyl chains and the move of branching positions that led to improved film morphology and PCEs of ~16.5%.[71, 72] An accompanying effect of these modifications is the enhanced solubility of the molecules, which enables device processing by non-halogenated solvent and printing-related techniques.[71, 73] Besides the inner side chains, more and more reports have demonstrated that the outer side chains may impose multiple effects on molecular conjugation, charge transport and electronic disorder, etc. By contrasting the acceptors with and without the outer side chains, So and Zou *et al*. discovered that these outer

chains endowed the molecules with lowered Urbach energy and energy disorder.[74] Zhan *et al*. also presented the replacement of alkyl chains with alkylphenyl groups to extend the conjugation and increase the intramolecular locking effects of the acceptors, which led to a comprehensive enhancement of the photovoltaic parameters.[75] Hou *et al*. carefully examined the length of the outer side chains by the interplay between solubility and electron transport, yielding an outstanding PCE of 17.8%.[76] These results have greatly advanced the development of nonfullerene OSCs, as it is undoubtedly intensive and delicate work to further improve the nearly optimum blend morphology of the Y-series NFAs. Nonetheless, current literatures focused on the alteration in the length, shape or branching positions of the outer side chains.[77] As these various side chains are connected with sp^2-hybridized atoms of the central DAD-cores, they mostly remain in the horizontal direction of the molecular backbone. Hence, it is interesting to explore if the side-chain orientations, specifically the extension direction of the chains relative to the molecular plane, can have impacts on intermolecular aggregation of the acceptors.

In this work, we study the effect of side-chain orientations on the properties and photovoltaic performances of Y-series NFAs. We designed and synthesized three isomeric NFAs,[78-80] named *o*-BTP-PhC6, *m*-BTP-PhC6, and *p*-BTP-PhC6, as shown in Fig. 1. The main structural difference of the three isomers is the substitution positions (i.e., *ortho*-, *meta*-, and *para*-substitutions) of the hexyl chains on the phenyl rings that are connected to the *β*-positions of the thienothiophene units, which allows us to systematically study the effects of side-chain orientations. As a result, morphology analysis and theoretical calculations revealed that the molecular geometry of various side chains can significantly alter the molecular aggregation, thereby affecting their physicochemical properties and electron mobilities of three NFAs. Consequently, when pairing with a wide-bandgap donor polymer PTQ10, these NFAs delivered different photovoltaic parameters. While *o*-BTP-PhC6 yielded only a moderate PCE of 16.0% due to an undesirable side-chain orientation, both *p*-BTP-PhC6 and *m*-BTP-PhC6 presented

PCEs exceeding 17% in binary devices. Importantly, *m*-BTP-PhC6 achieved an impressive PCE of 17.7%, due to the simultaneously increased short-circuit current density (J_{SC}) and fill factor (FF) relative to those of *p*-BTP-PhC6. As far as we know, this result represents one of the highest values among PTQ10-based OSCs, which sheds light on a new strategy of side-chain engineering for Y-series NFAs.

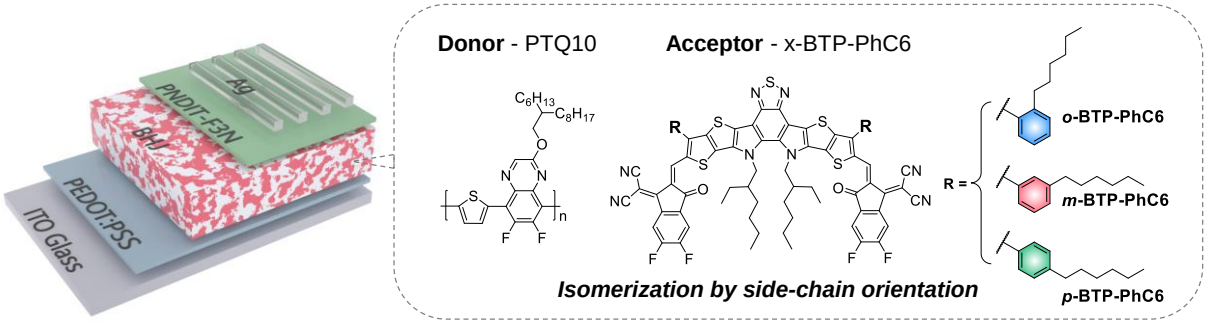

Fig. 1 Chemical structures of the donor polymer PTQ10 and the acceptor materials, *o*-BTP-PhC6, *m*-BTP-PhC6, and *p*-BTP-PhC6 developed in this work.

Results and Discussions

The detailed synthesis routes to *o*-BTP-PhC6, *m*-BTP-PhC6, and *p*-BTP-PhC6 are depicted in Scheme S1-3 in the Supporting Information (ESI†) with similar procedures. The only structural difference among these NFAs lies in the substitution positions (i.e., *ortho*-, *meta*-, and *para*-substitutions) of the hexyl chains on the phenyl rings attached to the *β*-positions of the thienothiophene units. All the three NFAs exhibit good solubility in common processing solvents including chloroform, toluene, and chlorobenzene. ^{1}H NMR, ^{13}C NMR, and MALDI-TOF techniques were utilized to characterize the chemical structures of the intermediates and final products with regioisomerism. The thermal properties of the three small molecules were characterized by thermogravimetric analysis (TGA). As shown in Fig. S1 in ESI†, *o*-BTP-PhC6, *m*-BTP-PhC6, and *p*-BTP-PhC6 exhibit decomposition temperature (T_d) with 5% weight loss at 311, 322, and 352 °C under nitrogen atmosphere, respectively. These results indicate that good solubility and thermal stability of the three NFAs are suitable for the applications in OSCs.

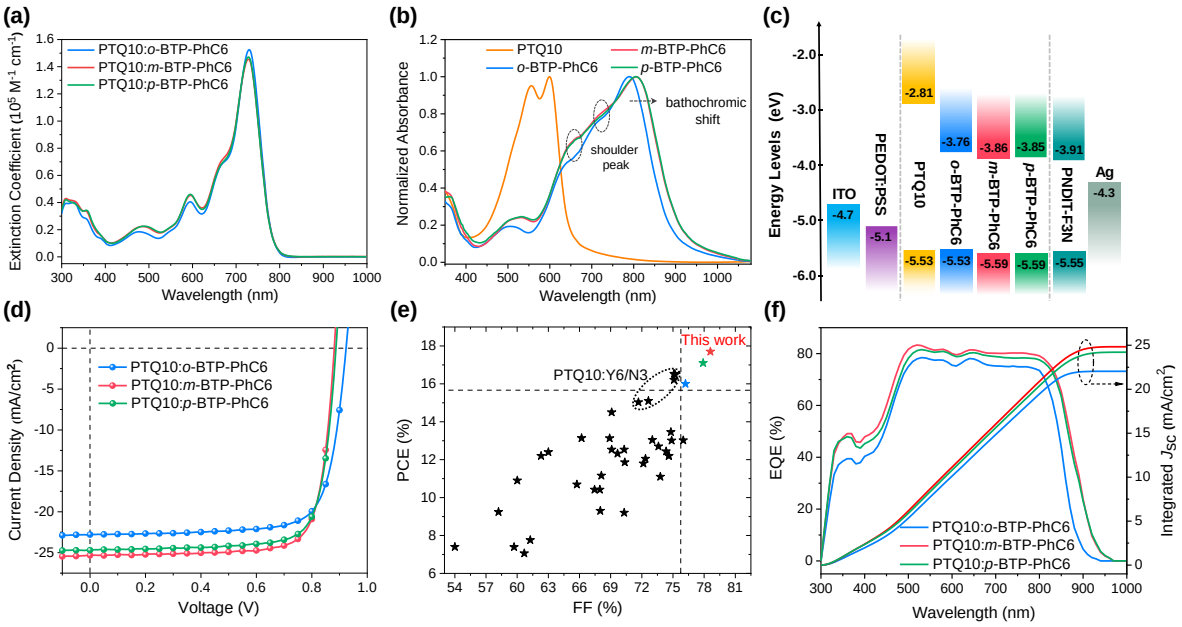

Fig. 2 (a) Absorption spectra of the three acceptors in chloroform solution with a concentration of ~1×10^{-5} M. (b) Normalized UV–vis absorption spectra of the donor and acceptors as thin films. (c) Energy level diagram of the related materials used in the OSC devices. (d) Optimized *J*-*V* curves under AM 1.5 G illumination. (e) Comparisons of the photovoltaic properties among PTQ10-based OSCs with representative FF and PCE values reported in the literature and this work. The dotted circle data represents the efficiencies of Y6 or N3 as the acceptor and the detailed parameters are collected in Table S1 (ESI†). (f) EQE curves of the corresponding optimized devices.

The ultraviolet−visible (UV−vis) absorption spectra of these isomeric NFAs were recorded in dilute chloroform solution with a concentration of ~1×10^{-5} M and in film state, and the corresponding optical data are listed in Table 1. As displayed in Fig. 2a, *o*-BTP-PhC6, *m*-BTP-PhC6, and *p*-BTP-PhC6 show similar absorption profiles ranging from of 300–780 nm with their maximum absorption peaks centered at 730, 728, and 728 nm, respectively. Together with their comparable extinction coefficients ($\varepsilon_{solution}$), it can be seen that the alkyl-substituted positions do not have a significant impact on the electronic structure of the resulting molecules

in solution. Whereas, when changing to the film state, the maximum absorption peaks show bathochromic shifts of 60, 78, and 77 nm for *o*-BTP-PhC6, *m*-BTP-PhC6, and *p*-BTP-PhC6, respectively (Fig. 2b). The obviously different bathochromic shifts of these films suggest that the side-chain orientations may have some influence on the molecular packing in these NFAs. The relative intensity of the shoulder peaks (at around 662 and 718 nm) also indicates the different extents of intermolecular aggregation for these NFAs. Besides, the optical bandgaps (E_g^{opt}) of *o*-BTP-PhC6, *m*-BTP-PhC6, and *p*-BTP-PhC6 calculated from their absorption onsets are 1.39, 1.35, and 1.36 eV, respectively. Since the absorption of polymer donor PTQ10 is mainly located in the range of 450–620 nm,[81] the complementary absorption of PTQ10 and three NFAs can provide wide and efficient absorption to construct OSCs, as shown in Fig. S2 (ESI†).

Table 1 The optical and electrochemical properties of *o*-BTP-PhC6, *m*-BTP-PhC6, and *p*-BTP-PhC6.

Acceptors	λ_{max} (nm)		$\varepsilon_{solution}$	$E_g^{opt\,a}$	HOMO/LUMO[b]	$E_g^{cv\,c}$
	Solution	Film	(10^5 M^{-1} cm^{-1})	(eV)	(eV)	(eV)
o-BTP-PhC6	730	790	1.53	1.39	−5.53/−3.76	1.77
m-BTP-PhC6	728	806	1.45	1.35	−5.59/−3.86	1.73
p-BTP-PhC6	728	805	1.47	1.36	−5.59/−3.85	1.74

[a] Estimated from the onset absorption of thin films $E_g^{opt} = 1240/\lambda_{onset}$; [b] Calculated from the onsets of reduction/oxidation potentials; [c] Calculated from $E_g^{CV} = E_{LUMO} - E_{HOMO}$.

The highest occupied molecular orbital (HOMO) and the lowest unoccupied molecular orbital (LUMO) energy levels of PTQ10 and the three NFAs were estimated via electrochemical cyclic voltammetry (CV) measurement. The energy diagram is presented in Fig. 2c, and the oxidation/reduction curves of the corresponding films are shown in Fig. S3

(ESI†). The E_{HOMO}/E_{LUMO} values of PTQ10, *o*-BTP-PhC6, *m*-BTP-PhC6, and *p*-BTP-PhC6 are calculated to be -5.53/-2.81, -5.53/-3.76, -5.59/-3.86, and -5.59/-3.85 eV, respectively. The changing tendency of the electrochemical bandgap (E_g^{CV}) for *o*-BTP-PhC6 is in accordance with its blue-shifted absorption in comparison with those of *m*-BTP-PhC6 and *p*-BTP-PhC6. In addition, the higher LUMO level of *o*-BTP-PhC6 would be favorable for achieving a higher open-circuit voltage (V_{OC}) in OSC devices. Therefore, these results show that alkyl chain substitutions on different positions of three isomers have a significant effect on their electrochemical properties.

Table 2 Summary the photovoltaic parameters of the optimized devices based on *o*-BTP-PhC6, *m*-BTP-PhC6, and *p*-BTP-PhC6 (1:1.2, *w*/*w*) under standard AM 1.5G illumination, 100 mW/cm^2.

Acceptors	V_{OC} (V)	J_{SC} (mA cm^{-2})	FF (%)	PCE (%) [a]
PTQ10:*o*-BTP-C6Ph	0.924 (0.920±0.002)	22.8 (22.5±0.21)	76.2 (74.3±1.49)	16.0 (15.6±0.23)
PTQ10:*m*-BTP-C6Ph	0.883 (0.878±0.003)	25.3 (24.8±0.26)	79.3 (77.4±1.21)	17.7 (17.3±0.22)
PTQ10:*p*-BTP-C6Ph	0.888 (0.882±0.002)	24.7 (24.3±0.20)	77.9 (75.3±1.29)	17.1 (16.7±0.24)

[a] Average values in brackets obtained from 20 devices.

A series of OSCs with the conventional device architecture of ITO/PEDOT:PSS/PTQ10:NFA/PNDIT-F3N (poly[(9,9-bis(3′-(*N*,*N*-dimethylamino)propyl)-2,7-fluorene)-*alt*-5,5′-bis(2,2′-thiophene)-2,6-naphthalene-1,4,5,8-tetracaboxylic-*N*,*N*′-di(2-ethylhexyl)imide])/Ag were fabricated to systematically assess the photovoltaic performance of *o*-BTP-PhC6, *m*-BTP-PhC6, and *p*-BTP-PhC6, where PNDIT-F3N was used to facilitate the electron extraction by alleviating the interfacial energy barriers,[82] and the detailed device parameters are recorded in Table S2-4 (ESI†). The PTQ10:NFA blends were spin-casted from the chloroform solution with an optimized weight ratio (1:1.2), a total concentration of ~20 mg

mL^{-1} and thermal annealing at 100 °C for 5 min. The typical current density-voltage (*J*-*V*) curves of the OSC devices are depicted in Fig. 2d, and the corresponding device parameters are listed in Table 2. Despite the highest V_{OC} of 0.924 V that matches well with the E_{LUMO} values, PTQ10:*o*-BTP-PhC6 only presents a relative low J_{SC} of 22.8 mA cm^{-2} and FF of 76.2%, which leads to a moderate PCE of 16.0%. In terms of PTQ10:*p*-BTP-PhC6, a PCE of 17.1% is realized along with a V_{OC} of 0.888 V, a J_{SC} of 24.7 mA cm^{-2}, and an FF of 77.9%, which is higher than the efficiency reported in our previous work obtained by PM6:*p*-BTP-PhC6.[75] Impressively, PTQ10:*m*-BTP-PhC6 realizes the highest J_{SC} of 25.3 mA cm^{-2} and FF of 79.3% among the three PTQ10-based devices, resulting in an outstanding PCE of 17.7%. Fig. S4 (ESI†) illustrates a histogram of efficiencies of 20 independent OSC devices for each blend. Obviously, the mean values of PCEs are progressively enhanced in the sequence of *o*-BTP-PhC6 (15.6%), *p*-BTP-PhC6 (16.7%), and *m*-BTP-PhC6 (17.3%). To the best of our knowledge, the superior PCEs of the PTQ10:*m*-BTP-PhC6 and PTQ10:*p*-BTP-PhC6 devices are among the highest values reported for PTQ10-based OSCs (Fig. 2e). The improved J_{SC} as well as FF are the main reasons for their high performances, and the mechanisms behind this are of great interest and significance as the only difference among these isomeric NFAs are their side-chain orientations.

Fig. 2f compares the external quantum efficiency (EQE) spectra of the three devices with *o*-BTP-PhC6, *m*-BTP-PhC6, and *p*-BTP-PhC6 as acceptors, respectively. Both devices based on *m*-BTP-PhC6 and *p*-BTP-PhC6 exhibit EQEs of over 75% in the range of 490-820 nm. And PTQ10:*m*-BTP-PhC6 shows a slightly higher response in the range of 350-900 nm with the maximum EQE of 83.3%. As a result, the integrated J_{SC} of PTQ10:*m*-BTP-PhC6 is higher than that of PTQ10:*p*-BTP-PhC6 (24.83 vs. 24.21 mA cm^{-2}). Conversely, PTQ10:*o*-BTP-PhC6 shows not only a narrow range of EQE due to the blue-shifted absorption, but also the lowest photon response with the highest EQE value of 78% that leads to an inferior integrated J_{SC} of 22.04 mA cm^{-2}. It has been demonstrated that a long exciton lifetime is one of the prerequisites for efficient charge generation in low-energy-offset OSC devices.[83] Therefore, time-resolved

photoluminescence (TRPL) experiments were performed to probe the singlet exciton lifetime of the three NFAs. From Fig. S5 **(**ESI†**)**, it is obvious that the pristine *m*-BTP-PhC6 film presents the longest singlet exciton lifetime, which should be one of the reasons for the highest EQE values of the *m*-BTP-PhC6 device. Similar phenomena can also be observed through femtosecond transient absorption spectroscopy (fsTA), where the kinetics of ground state bleaching (GSB, Fig. S6, ESI†) is the slowest for the pristine *m*-BTP-PhC6 film**.** Furthermore, steady-state photoluminescence (PL) quenching experiments were conducted (Fig. S7, ESI†), in which the donor and acceptor components were excited independently by the lasers with the wavelengths of 514 nm and 785 nm, respectively. The values of PL quenching excited at 514/785 nm are calculated to be 95.9/72.1%, 98.5/92.6%, and 98.3/89.2% for *o*-BTP-PhC6, *m*-BTP-PhC6, and *p*-BTP-PhC6, respectively. It is clear that PTQ10:*m*-BTP-PhC6 exhibits the most efficient hole and electron transfer while PTQ10:*o*-BTP-PhC6 shows the worst, which is consistent with their different EQE response and J_{SC} in the corresponding devices.

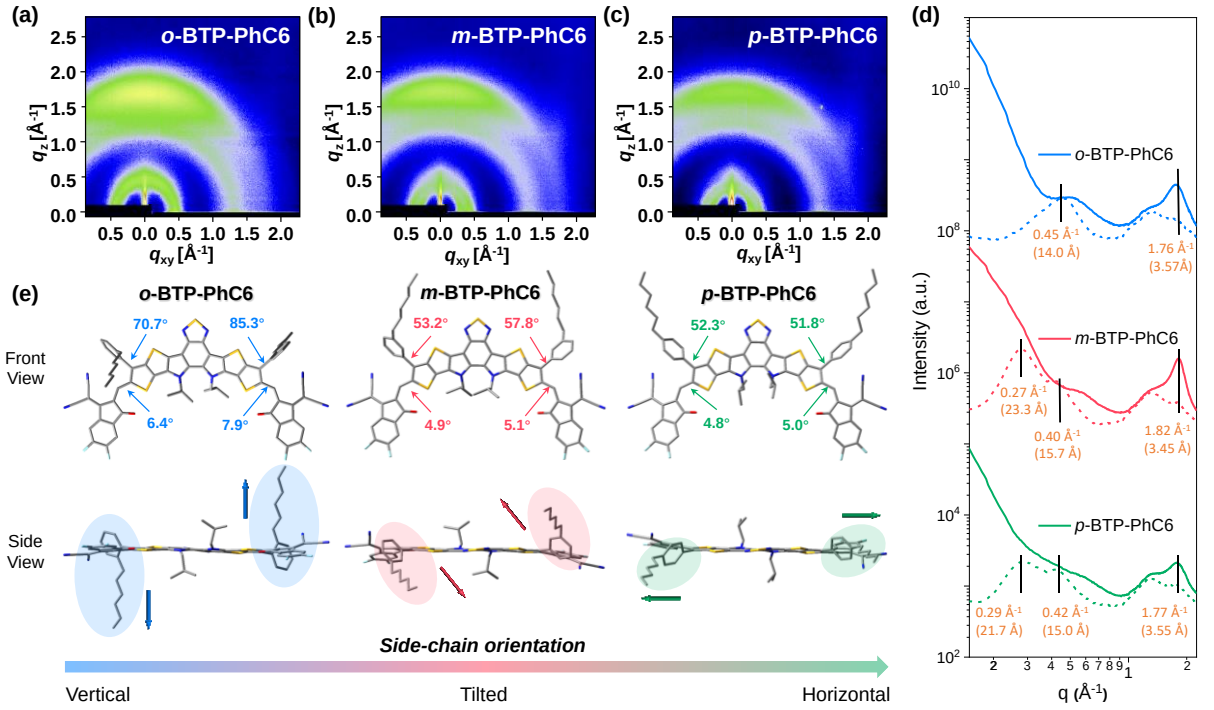

Fig. 3 GIWAXS patterns of (a) the pristine *o*-BTP-PhC6, (b) the pristine *m*-BTP-PhC6, and (c) the pristine *p*-BTP-PhC6 films. (d) Corresponding 1D scattering profiles of pristine films along

the in-plane (in dashed) and out-of-plane (in solid) directions. (e) DFT calculations of the optimized molecular geometry at B3LYP/6-31G(d,p) level of the three NFAs (hydrogen atoms are hidden for clarity). The 2-ethylhexyl chains attached to the pyrrole rings were replaced by 2-methylpropyl to accelerate the calculations.

To unravel the reasons why the side-chain orientations can affect the FF values of the NFAs, we first probed the thin-film morphology of the pristine NFAs by the grazing-incidence wide-angle X-ray scattering (GIWAXS) techniques.[84] The two-dimensional GIWAXS patterns (Fig. 3a-c) present all the (010) peaks of the three NFAs in the out-of-plane (OOP) direction, indicative of the preferentially face-on orientations relative to the substrate. The $\pi-\pi$ stacking distance ($d_{\pi\text{-}\pi}$) extracted from the corresponding one-dimensional profiles (Fig. 3d) are 3.57, 3.45, and 3.55 Å for *o*-BTP-PhC6, *m*-BTP-PhC6, and *p*-BTP-PhC6, respectively. *m*-BTP-PhC6 shows not only the shortest $d_{\pi\text{-}\pi}$ but also the largest crystal coherence length (CCL) of 2.8 nm compared to *o*-BTP-PhC6 (1.5 nm) and *p*-BTP-PhC6 (1.8 nm). In addition, from the in-plane (IP) direction, we can observe two lamellar stacking peaks at 0.27/0.40 $Å^{-1}$ for *m*-BTP-PhC6 (*d*-spacing: 23.3/15.7 Å) and 0.29/0.42 $Å^{-1}$ (*d*-spacing: 21.7/15.0 Å) for *p*-BTP-PhC6. By comparing the literature with detailed analysis of the single crystal and GIWAXS of Y6, these two lamellar peaks correspond to two different stacking patterns along the crystal axes that collectively form the two-dimensional network in the IP direction (instead of the linear polymer-like of ITIC-series NFAs).[62, 64, 85] In contrast, only one lamellar peak at 0.40 $Å^{-1}$ for *o*-BTP-PhC6 (*d*-spacing: 14.0 Å) can be found, which implies that the molecular packing of *o*-BTP-PhC6 may be different from those of Y6 and *m*-BTP-PhC6/*p*-BTP-PhC6. Accordingly, the disrupted molecular packing causes the blue-shifted absorption of *o*-BTP-PhC6 as mentioned before.

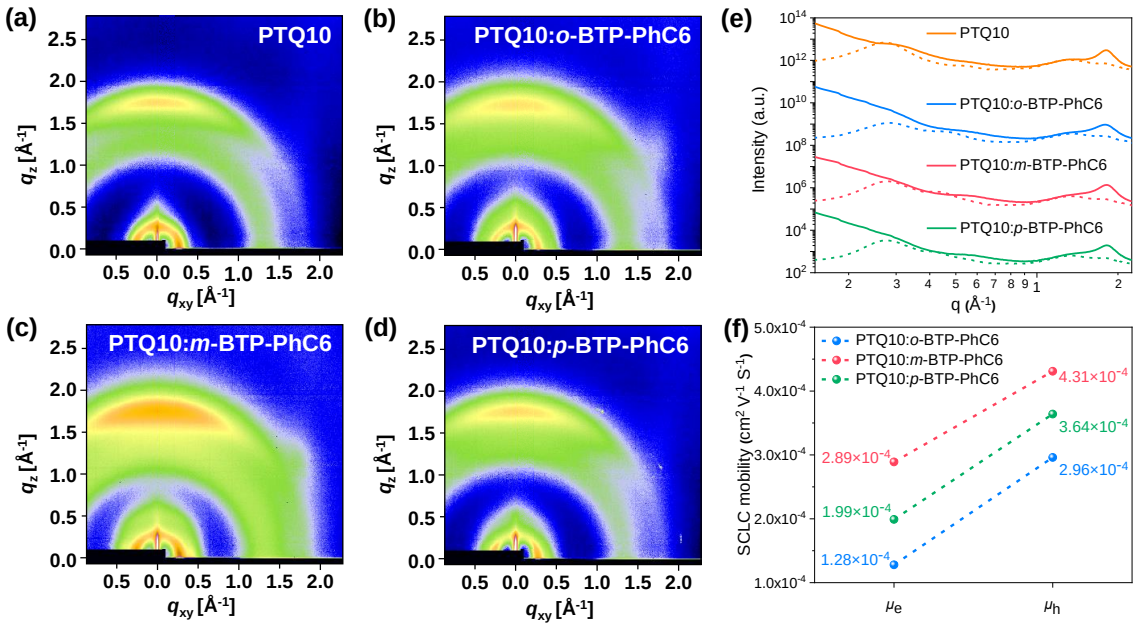

Fig. 4 2D GIWAXS patterns of (a) pristine PTQ10, (b) PTQ10:*o*-BTP-PhC6, (c) PTQ10:*m*-BTP-PhC6, and (d) PTQ10:*p*-BTP-PhC6 blend films. (e) Corresponding scattering profiles of blend films along the in-plane (in dashed) and out-of-plane (in solid) directions. (f) Hole and electron mobilities of the OSCs based on PTQ10:*o*-BTP-PhC6, PTQ10:*m*-BTP-PhC6, and PTQ10:*p*-BTP-PhC6.

It can be envisaged that the intermolecular packing of these molecules should be greatly altered by various side-chain orientations. Fig. 3e shows the density-functional theory (DFT) calculations of the optimized molecular geometry. From the side view, the hexyl chains of *o*-BTP-PhC6 point towards the vertical direction relative the molecular plane, which is in sharp contrast to those of *p*-BTP-PhC6 mostly sitting in the horizontal direction, and those of *m*-BTP-PhC6 adopting an in-between or "tilted" orientations. As for *o*-BTP-PhC6, it is speculated that the vertical orientation of the side chains can push away the neighbouring molecules, hampering the essential π-core stacking as evidenced by the missing lamellar peak.[25] Regarding the other two NFAs, *m*-BTP-PhC6 exhibits overall stronger intermolecular packing than *p*-BTP-PhC6, despite the larger dihedral angles in its molecular geometry. It should be noted that the shorter

$d_{\pi\text{-}\pi}$ of *m*-BTP-PhC6 may not be simply reduced to the steric hindrance from side chains. Although this interesting phenomenon should be investigated in the future by more precise methods such as single crystal or molecular-dynamics simulations, previous reports on ITIC-series NFAs also exemplify that the molecules with *meta*-positioned alkyl chains shows much stronger aggregation tendency than the isomers with *para*-positioned ones.[9] This is further supported by the electron mobility (μ_e) measurements by the space-charge-limited current (SCLC, Table S5 and Fig. S8**,** ESI†) method, where the μ_e for *o*-BTP-PhC6, *m*-BTP-PhC6, and *p*-BTP-PhC6 are 3.33×10^{-4}, 6.41×10^{-4}, and 5.23×10^{-4} cm^2 V^{-1} s^{-1}, respectively. Hence, these results strongly indicate that the side-chain orientations indeed have great impacts on the molecular packing properties and charge transport network of Y-series NFAs.

Furthermore, we wondered if these side-chain effects can be preserved in the nanostructure of the blend films and explain the differential device performance among these NFAs. The two-dimensional GIWAXS patterns of the pristine PTQ10 and the blend films are shown in Fig. 4a-d, and the corresponding one-dimensional profiles in the IP and OOP directions are plotted in Fig. 4e. It is discovered that blending NFAs with PTQ10 does not change the predominant face-on orientation for both donor and acceptor components. As tabulated in Table S6 (ESI†), the CCL values of the lamellar and $\pi-\pi$ stacking are estimated by Scherrer Equation to be 6.9 and 2.2 nm, 7.7 and 2.9 nm, and 8.0 and 2.7 nm for PTQ10:*o*-BTP-PhC6, PTQ10:*m*-BTP-PhC6, and PTQ10:*p*-BTP-PhC6, respectively. Since the PTQ10 diffraction signals are quite close to the blend films in the OOP direction, it is hard to precisely distinguish the contribution from donor or acceptor to the $\pi-\pi$ stacking scattering in blend films. However, the $\pi-\pi$ stacking scattering of the thin film containing *m*-BTP-PhC6 is found to be higher and shaper than those of other blend films, which indicates higher crystallinity and thicker crystals and accords with the information of the pristine films in the OOP direction. As the donor content in the thin films are the same, we can speculate that the higher crystallinity found here is from the acceptor *m*-BTP-PhC6. Again, the *o*-BTP-PhC6-based film shows the weakest crystallization propensity

relative to the other two material combinations, which is also supported by the SCLC mobility measurement of the blend film. As shown in Fig. 4f and Fig. S9 (ESI†), the blend films based on *o*-BTP-PhC6, *m*-BTP-PhC6, and *p*-BTP-PhC6 exhibit hole/electron mobility of $1.28\times10^{-4}/2.96\times10^{-4}$, $2.89\times10^{-4}/4.31\times10^{-4}$, and $1.99\times10^{-4}/3.64\times10^{-4}$ cm^2 V^{-1} s^{-1}, respectively. The GIWAXS and mobility results indicate that the PTQ10:*m*-BTP-PhC6 blend film possesses the strongest $\pi-\pi$ stacking and thus the highest charge mobility, which coincides the high J_{SC} and FF achieved in the devices.

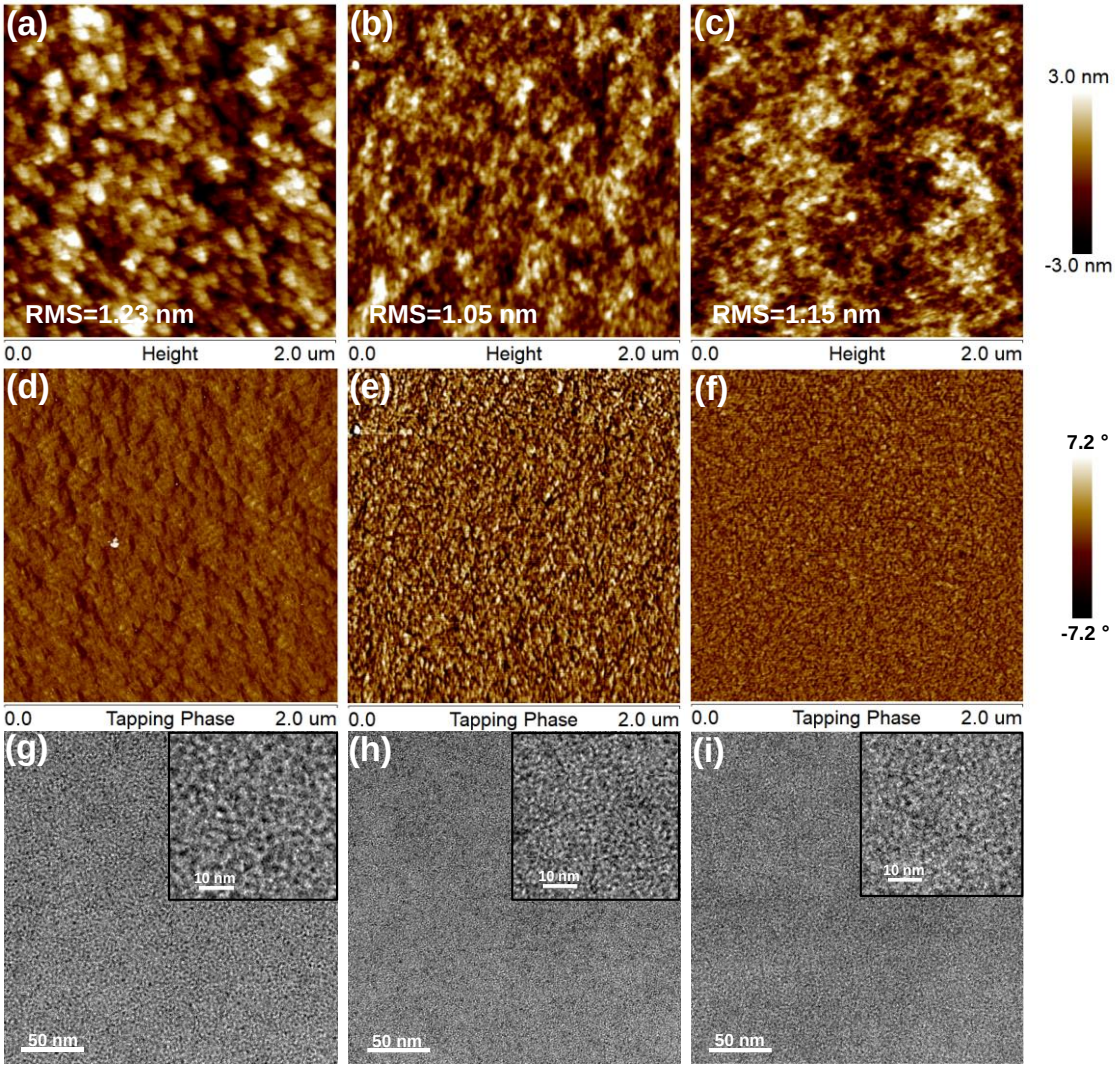

Fig. 5 (a-c) AFM height images, (d-e) AFM phase images and (g-i) TEM images (50 nm scale) of the PTQ10:*o*-BTP-PhC6, PTQ10:*m*-BTP-PhC6, and PTQ10:*p*-BTP-PhC6 blend films (the inserted scale bar is 10 nm).

Apart from molecular packing, we characterized the nanoscale phase separation of the blend films by employing atomic force microscopy (AFM) and transmission electron microscopy (TEM) to verify the effects of the side-chain orientations. As displayed in Fig. 5a-f, all the three blend films show uniform surfaces without the formation of undesirably large aggregates and relatively small root-mean-square (RMS) roughness are found to be approximately 1.0~1.2 nm, which is conducive to the efficient charge dissociation and collection. It should be noted that the PTQ10:*o*-BTP-PhC6 blend seems to have larger phase separation from the AFM images. To confirm this, TEM images were captured for these blends, where PTQ10:*o*-BTP-PhC6 (Fig. 5g) indeed shows increased phase separation compared to PTQ10:*m*-BTP-PhC6 and PTQ10:*p*-BTP-PhC6 (Fig. 5h and 5i). These results suggest that the large phase separation of PTQ10:*o*-BTP-PhC6 reduces the interfacial area between donor and acceptor, which may cause inefficient charge dissociation. On the contrary, the suitable phase separation of PTQ10:*m*-BTP-PhC6 and PTQ10:*p*-BTP-PhC6 provides more donor-acceptor interface for efficient charge dissociation to yield better J_{SC} and FF in the related devices.

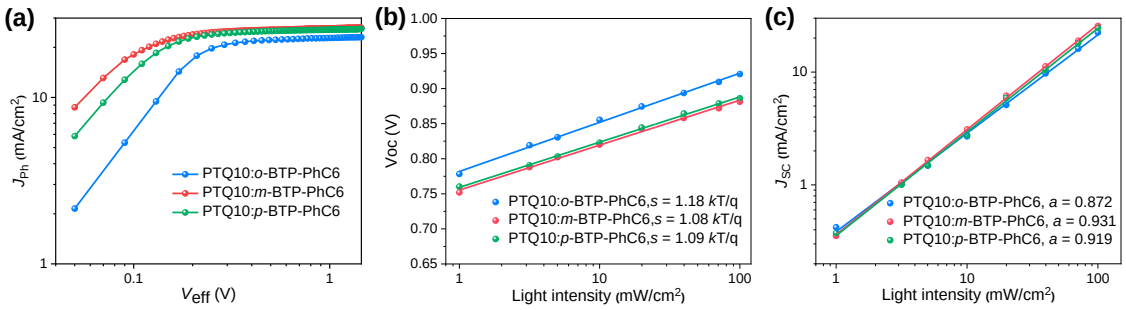

Fig. 6 (a) J_{ph} versus V_{eff} plots. (b) Light intensity dependence of V_{OC} and (c) light intensity dependence of J_{SC} of the PTQ10:*o*-BTP-PhC6, PTQ10:*m*-BTP-PhC6 and PTQ10:*p*-BTP-PhC6 devices.

To gain insight into the exciton dissociation and charge collection process, the plots of photocurrent density (J_{ph}) versus effective voltage (V_{eff}) of the three optimized devices were

studied (Fig. 6a and Table S7, ESI†). At a high V_{eff} of 2 V, all the devices reach their saturated photocurrent density (J_{sat}), suggesting that all the excitons are split and the resulting free charges are collected without recombination. It can be observed that the *m*-BTP-PhC6 and *p*-BTP-PhC6-based devices reached their J_{sat} at the relatively low V_{eff} compared to the *o*-BTP-PhC6 one. Theoretically, the exciton dissociation efficiency (η_{diss}) and charge collection efficiency (P_{coll}) can be estimated according to the formula of $\eta = J_{ph}/J_{sat}$ under the short circuit and maximum power point (MPP) conditions, respectively. PTQ10:*m*-BTP-PhC6 shows the highest η_{diss} and η_{coll} values (98.8% and 91.0%) compared with those of PTQ10:*o*-BTP-PhC6-based (95.8% and 87.0%) and PTQ10:*p*-BTP-PhC6-based devices (97.2% and 88.2%). These experiments demonstrate the trends in charge collection and exciton dissociation efficiencies are in accordance with those in J_{SC} and FF of the OSC devices and the TEM observations of their blend films.

Furthermore, by varying the light intensity (P_{light}) illuminated on the devices, we attempted to build up correlations between P_{light} and photovoltaic parameters (V_{OC} and J_{SC}) to investigate the charge recombination mechanisms. The plots of V_{OC} versus P_{light} in semi-logarithm coordinates are illustrated in Fig. 6b. A stronger dependence of V_{OC} and ln P_{light} with the slope > kT/q is considered to have more trap-assisted recombination, where k, T, and q denote Boltzmann constant, Kelvin temperature and elementary charge, respectively.[86] The calculated slopes for the *o*-BTP-PhC6, *m*-BTP-PhC6, and *p*-BTP-PhC6-based devices are 1.18 kT/q, 1.08 kT/q, and 1.09 kT/q, respectively. This implies that the major charge recombination for these three systems should be bimolecular recombination, with the *o*-BTP-PhC6-based device having more severe trap-assisted recombination. In addition, when the bimolecular recombination of the relevant device is negligible, the exponential factor α will approach unity in the formula of $J_{SC} \propto P_{light}^{\alpha}$.[87] As shown in Fig. 6c, the α values obtained from the slopes of the fitting lines are 0.872, 0.931, and 0.919 for the devices based on *o*-BTP-PhC6, *m*-BTP-PhC6, and *p*-BTP-PhC6,

respectively. The highest α value of the *m*-BTP-PhC6-based device indicates effectively suppressed bimolecular recombination, which accounts for its highest FF of >79%.

Conclusions

In summary, three isomeric NFAs named *o*-BTP-PhC6, *m*-BTP-PhC6, and *p*-BTP-PhC6 were rationally designed and synthesized by changing the side-chain substitution positions on the phenyl rings attached on the central core, and the impacts of the side-chain orientations on their optoelectronic and molecular aggregation properties were investigated. Relative to *o*-BTP-PhC6 with the vertical orientation and *p*-BTP-PhC6 with the horizontal orientation, the hexyl chains of *m*-BTP-PhC6 show a "tilted" orientation. Because of this unique orientation, *m*-BTP-PhC6 exhibits the most ordered intermolecular packing among three isomers, resulting in the enhanced electron mobility. When blended with PTQ10, the PCE of the *m*-BTP-PhC6-based devices reached 17.7% with a V_{OC} of 0.883 V, J_{SC} of 25.3 mA cm^{-2}, and FF of 79.3%, which is superior to those of the *o*-BTP-PhC6 (16.0%) and the *p*-BTP-PhC6-based ones (17.1%). Up to now, the PCE of 17.7% is among the highest efficiencies for the PTQ10-based OSCs reported in the literature. The suitable phase separation and enhanced molecular packing of PTQ10:*m*-BTP-PhC6 can effectively suppress the charge recombination and improve the charge transport, which is beneficial for the J_{SC} and FF of the devices. All these results demonstrate that fine-tuning the side-chain orientations plays a crucial role in altering the intermolecular aggregation properties of Y-series NFAs. Our work highlights the significance of the side-chain orientations as well as provides an alternative to the design of high-performance NFAs.

Author Contributions

G.C. and J.Z. designed, synthesized, and characterized the three isomeric NFAs. G.C., X.X., and L.Y. measured and analyzed the GIWAXS results. X.Z. and K.S.W. contributed to the TRPL, fsTA, and GSB measurements. J.Z. and Y.C. did the theoretical simulations. Y.C., S.L.,

F.B., H.Y., and T.L. performed the device fabrication and characterization of OSCs. Y.C., X.X., X.L., Y.C., Z.L., and H.Y. did the CV, AFM, and UV-vis absorption tests. B.L. and H.Z. carried out MS measurements. J.Z., Q.P., and H.Y. supervised the project. G.C., J.Z., and H.Y. wrote the paper.

Conflicts of interest

There are no conflicts to declare.

Acknowledgements

G.C., Y.C., and J.Z. contributed equally to this work. The work described in this paper was partially supported by the National Key Research and Development Program of China (No. 2019YFA0705900) funded by MOST, the Basic and Applied Basic Research Major Program of Guangdong Province (No. 2019B030302007), Guangdong-Hong Kong-Macao Joint Laboratory of Optoelectronic and Magnetic Functional Materials (project number 2019B121205002), the Shen Zhen Technology and Innovation Commission (project number JCYJ20170413173814007, JCYJ20170818113905024), the Hong Kong Research Grants Council (Research Impact Fund R6021-18, collaborative research fund C6023-19G, project numbers 16309218, 16310019, and 16303917), Hong Kong Innovation and Technology Commission for the support through projects ITC-CNERC14SC01 and ITS/471/18), National Natural Science Foundation of China (NSFC, No. 91433202). K.S.W. acknowledges the support from the Research Grants Council of Hong Kong (AoE/P-02/12). H.Z. acknowledges the support from National Natural Science Foundation of China (61974006), and Guangdong Natural Science Foundation (2018A030313332). The research used the Complex Materials Scattering (CMS) beamline of the National Synchrotron Light Source II (NSLS-II), which is an U.S. DOE Office of Science Facility, at Brookhaven National Laboratory under Contract No. DE-SC0012704.

Notes and references

1. S. Song, K. T. Lee, C. W. Koh, H. Shin, M. Gao, H. Y. Woo, D. Vak and J. Y. Kim, *Energy Environ. Sci.*, 2018, **11**, 3248-3255.
2. A. Wadsworth, M. Moser, A. Marks, M. S. Little, N. Gasparini, C. J. Brabec, D. Baran and I. McCulloch, *Chem. Soc. Rev.*, 2019, **48**, 1596-1625.
3. C. J. Brabec, A. Distler, X. Du, H. J. Egelhaaf, J. Hauch, T. Heumueller and N. Li, *Adv. Energy Mater.*, 2020, **10**, 2001864.
4. R. Sun, Q. Wu, J. Guo, T. Wang, Y. Wu, B. Qiu, Z. Luo, W. Yang, Z. Hu, J. Guo, M. Shi, C. Yang, F. Huang, Y. Li and J. Min, *Joule*, 2020, **4**, 407-419.
5. B. Lin, X. Zhou, H. Zhao, J. Yuan, K. Zhou, K. Chen, H. Wu, R. Guo, M. A. Scheel, A. Chumakov, S. V. Roth, Y. Mao, L. Wang, Z. Tang, P. Müller-Buschbaum and W. Ma, *Energy Environ. Sci.*, 2020, **13**, 2467-2479.
6. Y. Tong, Z. Xiao, X. Du, C. Zuo, Y. Li, M. Lv, Y. Yuan, C. Yi, F. Hao, Y. Hua, T. Lei, Q. Lin, K. Sun, D. Zhao, C. Duan, X. Shao, W. Li, H.-L. Yip, Z. Xiao, B. Zhang, Q. Bian, Y. Cheng, S. Liu, M. Cheng, Z. Jin, S. Yang and L. Ding, *Sci. China: Chem.*, 2020, **63**, 758-765.
7. D. Koo, S. Jung, J. Seo, G. Jeong, Y. Choi, J. Lee, S. M. Lee, Y. Cho, M. Jeong, J. Lee, J. Oh, C. Yang and H. Park, *Joule*, 2020, **4**, 1021-1034.
8. Y. Lin, J. Wang, Z. G. Zhang, H. Bai, Y. Li, D. Zhu and X. Zhan, *Adv. Mater.*, 2015, **27**, 1170-1174.
9. Y. Yang, Z. G. Zhang, H. Bin, S. Chen, L. Gao, L. Xue, C. Yang and Y. Li, *J. Am. Chem. Soc.*, 2016, **138**, 15011-15018.
10. G. Zhang, J. Zhao, P. C. Y. Chow, K. Jiang, J. Zhang, Z. Zhu, J. Zhang, F. Huang and H. Yan, *Chem. Rev.*, 2018, **118**, 3447-3507.
11. J. Hou, O. Inganas, R. H. Friend and F. Gao, *Nat. Mater.*, 2018, **17**, 119-128.

12. C. Yan, S. Barlow, Z. Wang, H. Yan, A. K. Y. Jen, S. R. Marder and X. Zhan, *Nat. Rev. Mater.*, 2018, **3**, 18003.

13. Z. Zhou, S. Xu, J. Song, Y. Jin, Q. Yue, Y. Qian, F. Liu, F. Zhang and X. Zhu, *Nat. Energy*, 2018, **3**, 952-959.

14. P. Cheng, G. Li, X. Zhan and Y. Yang, *Nat. Photonics*, 2018, **12**, 131-142.

15. L. Meng., Y. Zhang., X. Wan., C. Li., X. Zhang., Y. Wang., X. Ke., Z. Xiao., L. Ding., R. Xia., H.-L. Yip., Y. Cao. and Y. Chen., *Science*, 2018, **361**, 1094–1098.

16. J. Sun, X. Ma, Z. Zhang, J. Yu, J. Zhou, X. Yin, L. Yang, R. Geng, R. Zhu, F. Zhang and W. Tang, *Adv. Mater.*, 2018, **30**, 1707150.

17. H. Huang, Q. Guo, S. Feng, C. Zhang, Z. Bi, W. Xue, J. Yang, J. Song, C. Li, X. Xu, Z. Tang, W. Ma and Z. Bo, *Nat. Commun.*, 2019, **10**, 3038.

18. X. Chen, G. Xu, G. Zeng, H. Gu, H. Chen, H. Xu, H. Yao, Y. Li, J. Hou and Y. Li, *Adv. Mater.*, 2020, **32**, 1908478.

19. Q. Fan, W. Su, S. Chen, W. Kim, X. Chen, B. Lee, T. Liu, U. A. Méndez-Romero, R. Ma, T. Yang, W. Zhuang, Y. Li, Y. Li, T.-S. Kim, L. Hou, C. Yang, H. Yan, D. Yu and E. Wang, *Joule*, 2020, **4**, 658-672.

20. T. Jia, J. Zhang, W. Zhong, Y. Liang, K. Zhang, S. Dong, L. Ying, F. Liu, X. Wang, F. Huang and Y. Cao, *Nano Energy*, 2020, **72**, 104718.

21. S. Li, C.-Z. Li, M. Shi and H. Chen, *ACS Energy Lett.*, 2020, **5**, 1554-1567.

22. Z. Luo, R. Ma, T. Liu, J. Yu, Y. Xiao, R. Sun, G. Xie, J. Yuan, Y. Chen, K. Chen, G. Chai, H. Sun, J. Min, J. Zhang, Y. Zou, C. Yang, X. Lu, F. Gao and H. Yan, *Joule*, 2020, **4**, 1236-1247.

23. C. Zhu, J. Yuan, F. Cai, L. Meng, H. Zhang, H. Chen, J. Li, B. Qiu, H. Peng, S. Chen, Y. Hu, C. Yang, F. Gao, Y. Zou and Y. Li, *Energy Environ. Sci.*, 2020, **13**, 2459-2466.

24. L. Zhan, S. Li, T.-K. Lau, Y. Cui, X. Lu, M. Shi, C.-Z. Li, H. Li, J. Hou and H. Chen, *Energy Environ. Sci.*, 2020, **13**, 635-645.

25. F. Lin, K. Jiang, W. Kaminsky, Z. Zhu and A. K. Jen, *J. Am. Chem. Soc.*, 2020, **142**, 15246-15251.

26. T. Liu, R. Ma, Z. Luo, Y. Guo, G. Zhang, Y. Xiao, T. Yang, Y. Chen, G. Li, Y. Yi, X. Lu, H. Yan and B. Tang, *Energy Environ. Sci.*, 2020, **13**, 2115-2123.

27. Y. Lin, B. Adilbekova, Y. Firdaus, E. Yengel, H. Faber, M. Sajjad, X. Zheng, E. Yarali, A. Seitkhan, O. M. Bakr, A. El-Labban, U. Schwingenschlogl, V. Tung, I. McCulloch, F. Laquai and T. D. Anthopoulos, *Adv. Mater.*, 2019, **31**, 1902965.

28. Q. Yue, W. Liu and X. Zhu, *J. Am. Chem. Soc.*, 2020, **142**, 11613-11628.

29. J. Yao, B. Qiu, Z. G. Zhang, L. Xue, R. Wang, C. Zhang, S. Chen, Q. Zhou, C. Sun, C. Yang, M. Xiao, L. Meng and Y. Li, *Nat. Commun.*, 2020, **11**, 2726.

30. J. Yuan, Y. Q. Zhang, L. Y. Zhou, G. C. Zhang, H. L. Yip, T. K. Lau, X. H. Lu, C. Zhu, H. J. Peng, P. A. Johnson, M. Leclerc, Y. Cao, J. Ulanski, Y. F. Li and Y. P. Zou, *Joule*, 2019, **3**, 1140-1151.

31. B. B. Fan, D. F. Zhang, M. J. Li, W. K. Zhong, Z. M. Y. Zeng, L. Ying, F. Huang and Y. Cao, *Sci. China: Chem.*, 2019, **62**, 746-752.

32. J. Yuan, H. Zhang, R. Zhang, Y. Wang, J. Hou, M. Leclerc, X. Zhan, F. Huang, F. Gao, Y. Zou and Y. Li, *Chem*, 2020, **6**, 2147-2161.

33. Y. Cui, H. Yao, J. Zhang, T. Zhang, Y. Wang, L. Hong, K. Xian, B. Xu, S. Zhang, J. Peng, Z. Wei, F. Gao and J. Hou, *Nat. Commun.*, 2019, **10**, 2515.

34. Z. Zhou, W. Liu, G. Zhou, M. Zhang, D. Qian, J. Zhang, S. Chen, S. Xu, C. Yang, F. Gao, H. Zhu, F. Liu and X. Zhu, *Adv. Mater.*, 2020, **32**, 1906324.

35. S. Liu, J. Yuan, W. Deng, M. Luo, Y. Xie, Q. Liang, Y. Zou, Z. He, H. Wu and Y. Cao, *Nat. Photonics*, 2020, **14**, 300-305.

36. Z. Luo, R. Ma, Z. Chen, Y. Xiao, G. Zhang, T. Liu, R. Sun, Q. Zhan, Y. Zou, C. Zhong, Y. Chen, H. Sun, G. Chai, K. Chen, X. Guo, J. Min, X. Lu, C. Yang and H. Yan, *Adv. Energy Mater.*, 2020, **10**, 2002649.

37. X. Li, I. Angunawela, Y. Chang, J. Zhou, H. Huang, L. Zhong, A. Liebman-Peláez, C. Zhu, L. Meng, Z. Xie, H. Ade, H. Yan and Y. Li, *Energy Environ. Sci.*, 2020, DOI: 10.1039/d0ee02251a.

38. T. Liu, Y. Zhang, Y. Shao, R. Ma, Z. Luo, Y. Xiao, T. Yang, X. Lu, Z. Yuan, H. Yan, Y. Chen and Y. Li, *Adv. Funct. Mater.*, 2020, **30**, 2000456.

39. H. Yu, Z. Qi, J. Zhang, Z. Wang, R. Sun, Y. Chang, H. Sun, W. Zhou, J. Min, H. Ade and H. Yan, *J. Mater. Chem. A*, 2020, **8**, 23756-23765.

40. X. Xu, K. Feng, Z. Bi, W. Ma, G. Zhang and Q. Peng, *Adv. Mater.*, 2019, **31**, 1901872.

41. H. L. Sun, T. Liu, J. W. Yu, T. K. Lau, G. Y. Zhang, Y. J. Zhang, M. Y. Su, Y. M. Tang, R. J. Ma, B. Liu, J. E. Liang, K. Feng, X. H. Lu, X. G. Guo, F. Gao and H. Yan, *Energy Environ. Sci.*, 2019, **12**, 3328-3337.

42. Q. Liu, Y. Jiang, K. Jin, J. Qin, J. Xu, W. Li, J. Xiong, J. Liu, Z. Xiao, K. Sun, S. Yang, X. Zhang and L. Ding, *Sci. Bull.*, 2020, **65**, 272-275.

43. T. Wang, R. Sun, M. Shi, F. Pan, Z. Hu, F. Huang, Y. Li and J. Min, *Adv. Energy Mater.*, 2020, **10**, 2000590.

44. J. Wu, G. Li, J. Fang, X. Guo, L. Zhu, B. Guo, Y. Wang, G. Zhang, L. Arunagiri, F. Liu, H. Yan, M. Zhang and Y. Li, *Nat. Commun.*, 2020, **11**, 4612.

45. Y. Zhang, D. Liu, T. K. Lau, L. Zhan, D. Shen, P. W. K. Fong, C. Yan, S. Zhang, X. Lu, C. S. Lee, J. Hou, H. Chen and G. Li, *Adv. Funct. Mater.*, 2020, **30**, 1910466.

46. Y. Chang, T.-K. Lau, M.-A. Pan, X. Lu, H. Yan and C. Zhan, *Mater. Horizon.*, 2019, **6**, 2094-2102.

47. P. Cheng, H. C. Wang, R. Zheng, Y. Zhu, S. Dai, Z. Li, C. H. Chen, Y. Zhao, R. Wang, D. Meng, C. Zhu, K. H. Wei, X. Zhan and Y. Yang, *Adv. Mater.*, 2020, **32**, 2002315.

48. Q. An, J. Wang, X. Ma, J. Gao, Z. Hu, B. Liu, h. sun, X. Guo, X. L. Zhang and F. Zhang, *Energy Environ. Sci.*, 2020, DOI: 10.1039/d0ee02516j.

49. X. Xu, L. Yu, H. Yan, R. Li and Q. Peng, *Energy Environ. Sci.*, 2020, **13**, 4381-4388.

50. N. Gasparini, S. H. K. Paleti, J. Bertrandie, G. Cai, G. Zhang, A. Wadsworth, X. Lu, H.-L. Yip, I. McCulloch and D. Baran, *ACS Energy Lett.*, 2020, **5**, 1371−1379.

51. Y. Lin, Y. Firdaus, F. H. Isikgor, M. I. Nugraha, E. Yengel, G. T. Harrison, R. Hallani, A. El-Labban, H. Faber, C. Ma, X. Zheng, A. Subbiah, C. T. Howells, O. M. Bakr, I. McCulloch, S. D. Wolf, L. Tsetseris and T. D. Anthopoulos, *ACS Energy Lett.*, 2020, **5**, 2935-2944.

52. R. Ma, T. Liu, Z. Luo, K. Gao, K. Chen, G. Zhang, W. Gao, Y. Xiao, T.-K. Lau, Q. Fan, Y. Chen, L.-K. Ma, H. Sun, G. Cai, T. Yang, X. Lu, E. Wang, C. Yang, A. K. Y. Jen and H. Yan, *ACS Energy Lett.*, 2020, **5**, 2711-2720.

53. P. Cheng, J. Wang, X. Zhan and Y. Yang, *Adv. Energy Mater.*, 2020, **10**, 2000746.

54. K. Weng, L. Ye, L. Zhu, J. Xu, J. Zhou, X. Feng, G. Lu, S. Tan, F. Liu and Y. Sun, *Nat. Commun.*, 2020, **11**, 2855.

55. X. Du, Y. Yuan, L. Zhou, H. Lin, C. Zheng, J. Luo, Z. Chen, S. Tao and L. S. Liao, *Adv. Funct. Mater.*, 2020, **30**, 1909837.

56. Y. Wang, B. Jia, J. Wang, P. Xue, Y. Xiao, T. Li, J. Wang, H. Lu, Z. Tang, X. Lu, F. Huang and X. Zhan, *Adv. Mater.*, 2020, **32**, 2002066.

57. S. Xie, R. Xia, Z. Chen, J. Tian, L. Yan, M. Ren, Z. Li, G. Zhang, Q. Xue, H.-L. Yip and Y. Cao, *Nano Energy*, 2020, **78**, 105238.

58. X. Chen, Z. Jia, Z. Chen, T. Jiang, L. Bai, F. Tao, J. Chen, X. Chen, T. Liu, X. Xu, C. Yang, W. Shen, W. E. I. Sha, H. Zhu and Y. Yang, *Joule*, 2020, **4**, 1594-1606.

59. P. Xue, S. Dai, T.-K. Lau, J. Yu, J. Zhou, Y. Xiao, K. Meng, Z. Xie, G. Lu, X. Lu, R. P. S. Han and X. Zhan, *Sol. RRL*, 2020, **4**, 2000115.

60. A. Karki, J. Vollbrecht, A. L. Dixon, N. Schopp, M. Schrock, G. N. M. Reddy and T. Q. Nguyen, *Adv. Mater.*, 2019, **31**, 1903868.

61. L. Perdigon-Toro, H. Zhang, A. Markina, J. Yuan, S. M. Hosseini, C. M. Wolff, G. Zuo, M. Stolterfoht, Y. Zou, F. Gao, D. Andrienko, S. Shoaee and D. Neher, *Adv. Mater.*, 2020, **32**, 1906763.

62. L. Zhu, M. Zhang, G. Zhou, T. Hao, J. Xu, J. Wang, C. Qiu, N. Prine, J. Ali, W. Feng, X. Gu, Z. Ma, Z. Tang, H. Zhu, L. Ying, Y. Zhang and F. Liu, *Adv. Energy Mater.*, 2020, **10**, 1904234.

63. W. Zhu, A. P. Spencer, S. Mukherjee, J. M. Alzola, V. K. Sangwan, S. H. Amsterdam, S. M. Swick, L. O. Jones, M. C. Heiber, A. A. Herzing, G. Li, C. L. Stern, D. M. DeLongchamp, K. L. Kohlstedt, M. C. Hersam, G. C. Schatz, M. R. Wasielewski, L. X. Chen, A. Facchetti and T. J. Marks, *J. Am. Chem. Soc.*, 2020, **142**, 14532-14547.

64. G. Zhang, X. K. Chen, J. Xiao, P. C. Y. Chow, M. Ren, G. Kupgan, X. Jiao, C. C. S. Chan, X. Du, R. Xia, Z. Chen, J. Yuan, Y. Zhang, S. Zhang, Y. Liu, Y. Zou, H. Yan, K. S. Wong, V. Coropceanu, N. Li, C. J. Brabec, J. L. Bredas, H. L. Yip and Y. Cao, *Nat. Commun.*, 2020, **11**, 3943.

65. X. Zhu, G. Zhang, J. Zhang, H.-L. Yip and B. Hu, *Joule*, 2020, **4**, 2443-2457.

66. Y. Cui, H. Yao, L. Hong, T. Zhang, Y. Tang, B. Lin, K. Xian, B. Gao, C. An, P. Bi, W. Ma and J. Hou, *Natl. Sci. Rev.*, 2020, **7**, 1239-1246.

67. D. Mo, H. Chen, J. Zhou, N. Tang, L. Han, Y. Zhu, P. Chao, H. Lai, Z. Xie and F. He, *J. Mater. Chem. A*, 2020, **8**, 8903-8912.

68. H. Wang, T. Liu, J. Zhou, D. Mo, L. Han, H. Lai, H. Chen, N. Zheng, Y. Zhu, Z. Xie and F. He, *Adv. Sci.*, 2020, **7**, 1903784.

69. H. Yu, R. Ma, Y. Xiao, J. Zhang, T. Liu, Z. Luo, Y. Chen, F. Bai, X. Lu, H. Yan and H. Lin, *Mater. Chem. Front.*, 2020, **4**, 2428-2434.

70. G. Chai, J. Zhang, M. Pan, Z. Wang, J. Yu, J. Liang, H. Yu, Y. Chen, A. Shang, X. Liu, F. Bai, R. Ma, Y. Chang, S. Luo, A. Zeng, H. Zhou, K. Chen, F. Gao, H. Ade and H. Yan, *ACS Energy Lett.*, 2020, **5**, 3415−3425.

71. L. Hong, H. Yao, Z. Wu, Y. Cui, T. Zhang, Y. Xu, R. Yu, Q. Liao, B. Gao, K. Xian, H. Y. Woo, Z. Ge and J. Hou, *Adv. Mater.*, 2019, **31**, 1903441.

72. K. Jiang, Q. Y. Wei, J. Y. L. Lai, Z. X. Peng, H. Kim, J. Yuan, L. Ye, H. Ade, Y. P. Zou and H. Yan, *Joule*, 2019, **3**, 3020-3033.

73. S. Dong, T. Jia, K. Zhang, J. Jing and F. Huang, *Joule*, 2020, **4**, 2004-2016.

74. C. Zhang, J. Yuan, K. L. Chiu, H. Yin, W. Liu, G. Zheng, J. K. W. Ho, S. Huang, G. Yu, F. Gao, Y. Zou and S. K. So, *J. Mater. Chem. A*, 2020, **8**, 8566-8574.

75. G. Chai, Y. Chang, Z. Peng, Y. Jia, X. Zou, D. Yu, H. Yu, Y. Chen, P. C. Y. Chow, K. S. Wong, J. Zhang, H. Ade, L. Yang and C. Zhan, *Nano Energy*, 2020, **76**, 105087.

76. Y. Cui, H. Yao, J. Zhang, K. Xian, T. Zhang, L. Hong, Y. Wang, Y. Xu, K. Ma, C. An, C. He, Z. Wei, F. Gao and J. Hou, *Adv. Mater.*, 2020, **32**, 1908205.

77. X. Li, H. Huang, I. Angunawela, J. Zhou, J. Du, A. Liebman-Pelaez, C. Zhu, Z. Zhang, L. Meng, Z. Xie, H. Ade and Y. Li, *Adv. Funct. Mater.*, 2019, **30**, 1906855.

78. Z. Luo, T. Liu, H. Yan, Y. Zou and C. Yang, *Adv. Funct. Mater.*, 2020, **30**, 2004477.

79. T. Li, Y. Wu, J. Zhou, M. Li, J. Wu, Q. Hu, B. Jia, X. Pan, M. Zhang, Z. Tang, Z. Xie, T. P. Russell and X. Zhan, *J. Am. Chem. Soc.*, 2020, **142**, 20124-20133.

80. J. Wang, J. Zhang, Y. Xiao, T. Xiao, R. Zhu, C. Yan, Y. Fu, G. Lu, X. Lu, S. R. Marder and X. Zhan, *J. Am. Chem. Soc.*, 2018, **140**, 9140-9147.

81. C. Sun, F. Pan, H. Bin, J. Zhang, L. Xue, B. Qiu, Z. Wei, Z. G. Zhang and Y. Li, *Nat. Commun.*, 2018, **9**, 743.

82. Z. Wu, C. Sun, S. Dong, X. F. Jiang, S. Wu, H. Wu, H. L. Yip, F. Huang and Y. Cao, *J. Am. Chem. Soc.*, 2016, **138**, 2004-2013.

83. A. Classen, C. L. Chochos, L. Lüer, V. G. Gregoriou, J. Wortmann, A. Osvet, K. Forberich, I. McCulloch, T. Heumüller and C. J. Brabec, *Nat. Energy*, 2020, **5**, 711-719.

84. A. Hexemer, W. Bras, J. Glossinger, E. Schaible, E. Gann, R. Kirian, A. MacDowell, M. Church, B. Rude and H. Padmore, *J. Phys. Conf. Ser.*, 2010, **247**, 012007.

85. J. Mai, Y. Xiao, G. Zhou, J. Wang, J. Zhu, N. Zhao, X. Zhan and X. Lu, *Adv. Mater.*, 2018, **30**, 1802888.

86. L. J. A. Koster, V. D. Mihailetchi, R. Ramaker and P. W. M. Blom, *Appl. Phys. Lett.*, 2005, **86**, 123509.

87. P. Schilinsky, C. Waldauf and C. J. Brabec, *Appl. Phys. Lett.*, 2002, **81**, 3885-3887.

Fine-tuning of Side-chain Orientations on Nonfullerene Acceptors Enables Organic Solar Cells with 17.7% Efficiency

Gaoda Chai,‡[ab] Yuan Chang,‡[ab] Jianquan Zhang,*‡[ab] Xiaopeng Xu,[c] Liyang Yu,[c] Xinhui Zou,[abd] Xiaojun Li,[ab] Yuzhong Chen,[ab] Siwei Luo,[ab] Binbin Liu,[e] Fujin Bai,[ab] Zhenghui Luo,[ab] Han Yu,[ab] Jiaen Liang,[ab] Tao Liu,[ab] Kam Sing Wong,[d] Hang Zhou,[e] Qiang Peng*[c] and He Yan*[abf]

Keywords: organic solar cells, non-fullerene acceptors, side-chain orientation, isomerization

ToC figure:

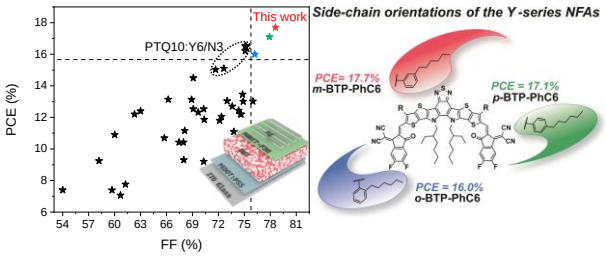

Regulating side-chain orientations of Y-series NFAs is a promising strategy to achieve favorable morphology, high charge mobility and solar cell performances, which enables high-performance devices with efficiency approaching 18%.